Active Thermal Management for Enhancing Peak-Current Capability of Three-Phase Inverters

Christoph H. van der Broeck*, Rik W. De Doncker*
*Institute for Power Electronics and Electrical Drives (ISEA), RWTH Aachen University
Jaegerstrasse 17-19, 52066 Aachen, Germany, Email: post@isea.rwth-aachen.de

***Abstract*—This work proposes an active thermal management for three-phase IGBT-based inverters that estimates adaptively the maximal feasible peak current and operates the inverter safely at enhanced peak current rating. The active thermal management only requires processing a compact electrothermal real-time model and NTC-temperature information. Thus, it is applicable on most state-of-the art drive systems with small software modifications. The introduced method uses two technologies to increase the peak power rating dynamically: First, it estimates the coolant and junction temperature to adaptively determine the maximal peak current capability that increases at low coolant temperature. Second, it takes advantage of the thermal-impedance frequency-response function $Z_{\mathrm{th}}(j\omega)$ that decays with higher frequencies in almost all power modules. This effect allows operation with larger peak current and the associated losses at higher excitation frequencies without exceeding the maximal junction temperature. With the introduced method, state-of-the-art drive inverters can operate safely at up to 200 % overload current across a wide speed range. This supports the development of highly reliable drives with increased base speed range and power density that save space, cost and resources.**

I. Introduction

In the development of power electronic systems, there exists a strong demand for improved power density as well as cost and resource efficiency [1]–[3]. Over the last decade, much research addressed this demand such that nowadays converters use advanced semiconductor devices [4], [5], packaging and assembly technologies [6]–[8], condition monitoring [9]–[12] and thermal management concepts [1], [13], [14] to realize highly integrated power conversion systems.

In recent years, active thermal management and control systems started to play a role in this development [15], [16]. They control thermal stress in power converters by manipulating converter current [16], [17], switching frequency [18]–[20], switching transients [21]–[23], heat dissipation [24], [25] or modulation schemes [26]. Thereby, power converters can be operated more closely to their thermal limits [16], [17] and thermal cycles and thus fatigue is reduced [27]. There exist two major types of active thermal control systems: Open loop thermal control methods only adjust the manipulated input as a function of the converter operation point allowing a simple implementation [18], [20], [28]. Closed loop thermal control technologies extract power module temperature information, e.g. coolant temperature [29] or even junction temperature [30]–[34] to estimate relevant thermal control variables [35], [36]. These are consequently used to manipulate the aforementioned manipulated inputs such that the thermal control variables follow a desired trajectory [16], [19], [27]. This improves the robustness and accuracy of the thermal control, but requires a more complex implementation. The key ideas that motivated state-of-the-art research in active thermal management are:

- Reducing thermal cycles to increase the life time of power converters, e.g. [16], [18], [20], [24], [27], [37]
- Equalizing stress in converter components to prevent unbalanced aging [23], [28], [38]
- Preventing thermal over-load by actively controlling converter operation [16], [17], [19]

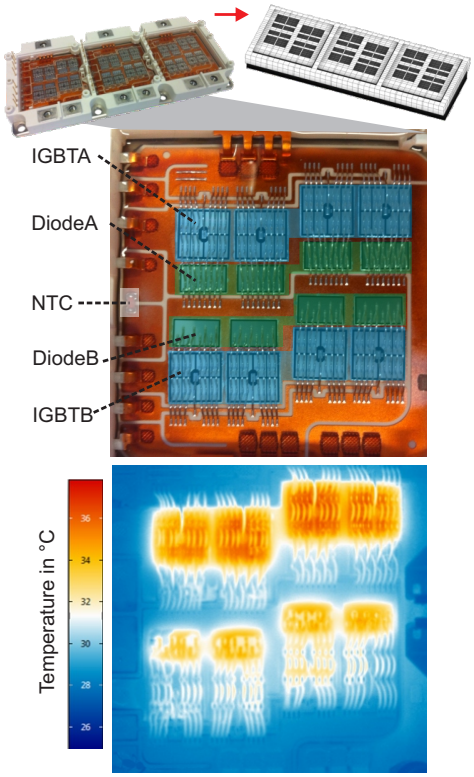

Fig. 1. Images and 3-D thermal finite-volume model of the Hybridpack2 (top) and IR image of power module during operation (bottom)

The authors, Christoph H. van der Broeck and Rik W. De Doncker, would like to thank the Institute for Power Electronics and Electrical Drives (ISEA) at RWTH Aachen University for supporting this research. This work was funded by the German Federal Ministry of Education and Research (BMBF) within the project ZuLeSELF funded according to a resolution of the German Federal Parliament (BMBF, Support Code 16EMO0324).

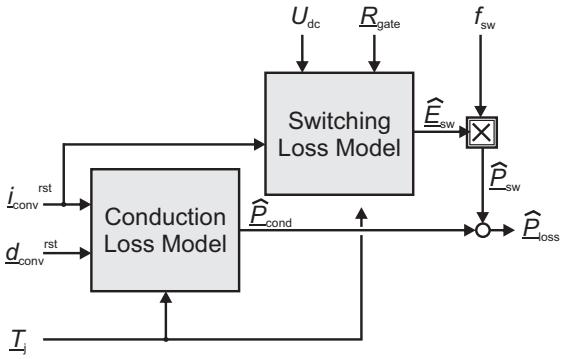

Fig. 2. State block diagram of the parametric loss model

However, opportunities that have been barely addressed yet lie in developing active thermal management that increases the power rating of power electronics without effecting converter operation. This provides a great potential for further integration of future converters systems, as it allows downsizing converters in size, weight, costs and resources without compromising reliability. This paper investigates such opportunities for IGBT-based three-phase inverter modules in electrical drives. Drive inverters are typically operated with a static peak current $I_{\mathrm{r}}^{\max}$. The peak current rating is determined during the design of the converter on the basis of the thermal resistance R_{th}, the maximal devices losses $P_{\mathrm{loss}}^{\max}$, the maximal junction temperature $T_{\mathrm{j}}^{\max}$ and the coolant temperature T_{f} [39]. This *passive design* ensures that the power module is never operated above the maximal permissible junction temperature $T_{\mathrm{j}}^{\max}$. However, the assembly of most IGBT-based power modules that are used in drive applications intrinsically provides features for active thermal management that can dynamically increase the current rating at many operation points. This is possible when the drive train operates at higher excitation frequencies or when the coolant temperature is low. In both situations, the converter assembly can operate with an elevated current limit compared to a worst case operation point, i.e. operation at maximal coolant temperature or with dc-currents. To address this opportunity, a new technology is proposed that utilizes thermal monitoring and dynamic peak current control to adaptively determine the maximal converter current that can be safely realized. It is shown how this *active design* yields a strong integration of future drive trains; saving space, costs and resources; without compromising reliability or safety.

The paper starts by presenting the key components that are required for the thermal monitoring and active thermal management system, i.e. a thermal model and NTC temperature information. Consequently, the thermal monitoring algorithm is reviewed that estimates junction temperature, 3-D distributed temperatures as well as the coolant temperature. Then, the paper proposes an active thermal management that adaptively determines and controls the maximal current at which the converter can safely operate. The advantages of the introduced active thermal management is exemplary demonstrated by comparing the torque capability of an electrical drive with and with and without peak current control. This comparison shows

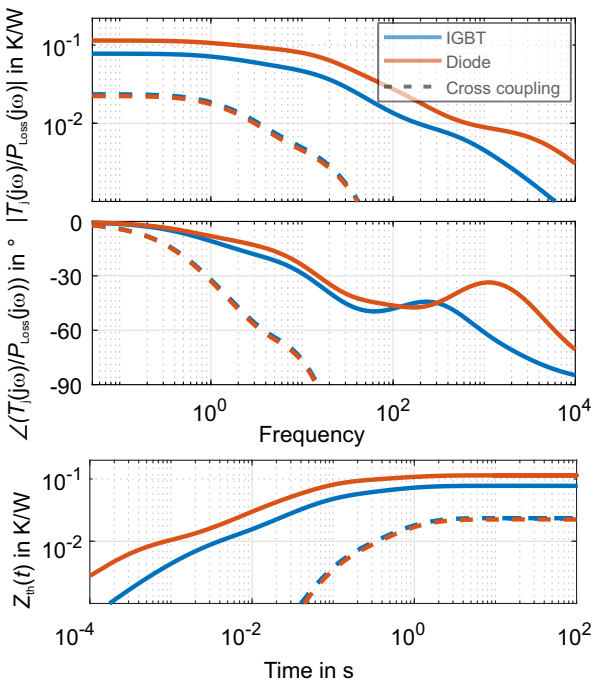

Fig. 3. Thermal impedance response of the Hybridpack2 power module obtained from a 3-D finite difference model. A) The upper two plot shows the frequency response function $Z_{\mathrm{th}}(j\omega)$ in magnitude and phase. B) The lower plot shows the transient thermal impedance $Z_{\mathrm{th}}(t)$, i.e. the thermal step response, plotted in the time domain

that the active thermal management allows applying smaller power modules for drive application without reducing the peak power rating of the drive train. The final section presents and discusses experimental results that demonstrate the feasibility of the introduced concept.

II. Thermal Real-Time Modeling and Sensors

This section reviews thermal real-time models as well as sensors for implementing the active thermal management.

A. Thermal Real-Time Model

One key component for the active thermal management solution is a compact thermal real-time models that computes the junction temperatures of the power devices as well as the NTC-temperature. The electrothermal real-time model used in this work applies a state-of-the-art parametric device loss model, whose structure is depicted in Fig. 2 It determines the switching-period averaged losses $\underline{\hat{P}}_{\mathrm{loss}}$ as a function of the converter currents $\underline{i}_{\mathrm{conv}}^{\mathrm{rst}}$ the duty cycles $\underline{d}_{\mathrm{conv}}^{\mathrm{rst}}$, the dc-link voltage U_{dc}, the applied gate resistances $\underline{R}_{\mathrm{gate}}$, the junction temperatures of the devices $\underline{T}_{\mathrm{j}}$ and the switching frequency f_{sw}. The parametric equation as well as the parameters that were obtained to calibrate the model for the Hybridpack2 power module are summarized in [35].

A compact thermal real-time model computes the junction temperatures of the power devices as well as the NTC-temperature on the basis of the device losses. It is obtained by 3-D finite volume modeling and model-order reduction using the balanced truncation method [40], [41]. The entire modeling

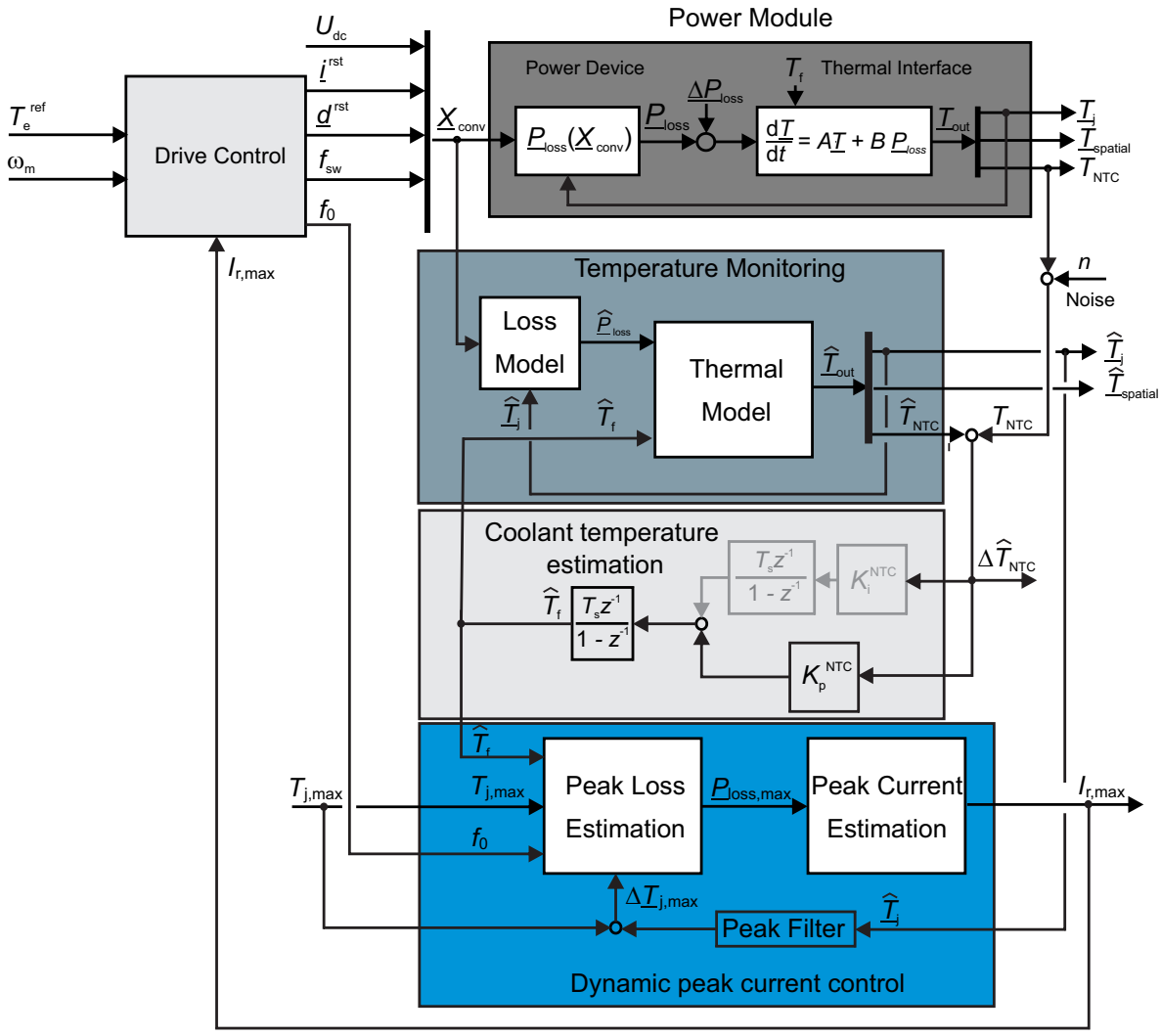

Fig. 4. State block diagram of the active thermal management system that comprises a temperature monitoring unit, a coolant temperature estimation and a dynamic peak current control

procedure has been analyzed in depth and utilized in various real-time application, e.g. in [36], [42]–[44]. The resulting model is a state-space model that determines the temperatures of the devices and the NTC, which are embedded in the vector $\underline{T}$ as a function of the devices losses $\underline{P}_{\text{loss}}$. It is given for one half-bridge according to (2).

$$\frac{\mathrm{d}\underline{x}}{\mathrm{d}t} = \mathbf{A}\cdot\underline{x} + \mathbf{B}\cdot\underline{P}_{\text{loss}} \qquad \underline{T} = \mathbf{C}\cdot\underline{x} \tag{1}$$

$$\underline{T} = \begin{pmatrix} T_{\text{j}}^{\text{IGBTA}} & T_{\text{j}}^{\text{DiodeA}} & T_{\text{j}}^{\text{IGBTB}} & T_{\text{j}}^{\text{DiodeB}} & T_{\text{j}}^{\text{NTC}} \end{pmatrix}' \tag{2}$$

In case of the Hybridpack2 power module, which is used as an example in this work, the introduced modeling approach takes into account the heat flow in the finite-volume model illustrated in Fig. 1. It computes the temperatures of the IGBTs and diodes as well as the temperature at the location of the NTC. The thermal impedance of the devices in the Hybridpack2, which were obtained with the model, are shown in Fig. 3. The frequency response function plot, which is in-depth discussed in [45], [46], shows the magnitude and phase of the thermal response as well as their cross coupling to periodic loss excitation. The second plot shows the transient thermal impedance of the devices, which can be found in any data-sheet. For the following derivation of the active thermal management, one needs the introduced frequency domain model information and any thermal real-time model that computes junction and NTC temperature. Both can alternatively be derived based on data-sheet information, e.g. using Cauer- or Foster-models [46] that calculate junction and NTC temperature.

B. NTC-Based Temperature Measurement

The second information that is required for ensuring accurate monitoring is measured temperature data from inside the power module. Without this information the junction temperatures are predicted open loop such that errors of the

thermal model as well as drifts in the coolant temperature are not compensated. In recent years, many technologies have been proposed that extract temperatures at different locations of power module. Most advanced solutions yield the extraction of junction temperature information via temperature-sensitive electrical parameters [31], [33], [47], on-chip temperature sensors [48] or temperature-sensitive optical parameters [34], [49]. This allows the effective real-time estimation of 3-D distributed temperatures throughout the power module on the basis of developed monitoring algorithms [36], [50] However, the vast majority of power modules in real-world applications only exhibits a thermistor that is attached to the substrate, e.g. a nonlinear temperature coefficient thermistor (NTC). The location of the NTC at the proximity of the substrate, which is depicted in Fig. 1, only allows extracting temperature information of the substrate and the heat sink. This can be effectively observed in the IR image of the decapsulated Hybridpack2 power module during operation and is in-depth investigated in [29]. For reconstructing the device temperature from the NTC temperature data, an observer-based monitoring approach becomes necessary, which is introduced in the following.

III. Thermal Monitoring of Power Modules

This work utilizes the thermal monitoring approach that has been developed in [29]. The state-block diagram of the thermal monitoring system that consists of the temperature monitoring unit and the coolant temperature estimation is depicted in Fig. 4. It requires the converter operation vector $\underline{X}_{\mathrm{conv}}$ as an input that is commanded by the drive control to realize a desired torque command $T_{\mathrm{e}}^{\mathrm{ref}}$. In a first step, an empirical loss model in the temperature monitoring unit estimates the device losses $\underline{\hat{P}}_{\mathrm{loss}}$ based on [41]. The devices losses and a coolant temperature estimate $\hat{T}_{\mathrm{f}}$ are consequently fed to the thermal real-time model (2) to estimate temperatures at the devices T_{j} and at the NTC T_{NTC}. The estimated NTC temperature is compared with the measurement and the error is processed by a proportional-integral (PI) regulator to correct the coolant temperature estimate. This structure allows adaptively estimating the coolant temperature T_{f} of the power module, such that the thermal real-time model can estimate the junction temperatures with good precision even if fast changes of T_{f} occur. Furthermore, this structure can detect structural changes of the heat dissipation path between substrate and heat sink, e.g. due to solder delamination. By compensating their effect with a higher coolant temperature, it makes sure that this degradation do not strongly mitigate the junction temperature estimation. A more detailed discussion of this monitoring structure can be found in [29] that also includes experimental results to demonstrate how this approach estimates coolant temperature and junction temperature with good accuracy every millisecond on a normal DSP.

IV. Active Thermal Management

This section analyses the junction temperature response T_{j} at different excitation frequencies and uses the obtained results to develop an effective active thermal management.

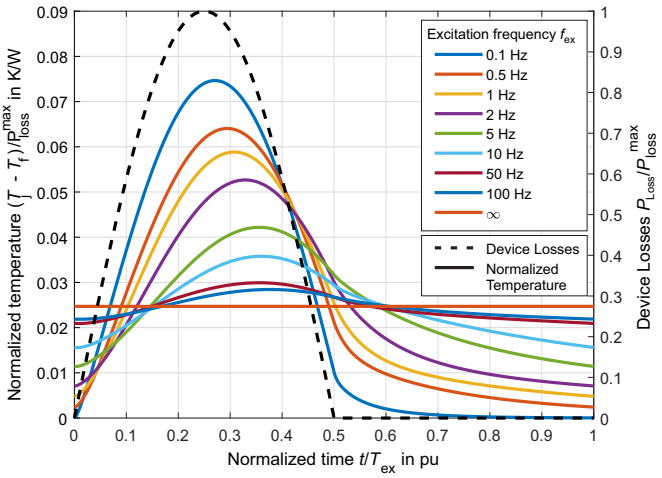

Fig. 5. Normalized temperature response of the junction T_{j} to sinusoidal half-wave loss excitation with the amplitude $P_{\mathrm{loss}}^{\mathrm{max}}$ at a wide range of excitation frequencies $f_{\mathrm{ex}} = 1/T_{\mathrm{ex}}$

A. Response of T_{j} at Different Excitation Frequencies

For keeping the analysis and thus the active thermal management simple, the following two assumptions are made. They apply for a majority of inverters over a wide operation range, most importantly close to thermal limits:

1 The thermal cross-coupling between the IGBTs and the diodes is negligible: $|Z_{\mathrm{th}}^{\mathrm{ii}}(j\omega)| >> |Z_{\mathrm{th}}^{\mathrm{ij}}(j\omega)|$.
2 IGBTs show higher maximal temperatures compared to diodes $T_{\mathrm{j}}^{\mathrm{IGBT,max}} >> T_{\mathrm{j}}^{\mathrm{Diode,max}}$.
3 The losses that occur over one electrical excitation period f_{ex} follow a sinusoidal half-wave, i.e. as given by (3)

The first assumption is true for most power modules, as lateral heat dissipation paths mitigates thermal cross-coupling. Fig. 3 shows its validity for the Hybridpack2 power module. The second assumption holds, because the conduction losses dominantly occur in the IGBT for $\cos(\varphi) > 0$ and the switching losses in the diode are negligible. As a consequence of the first and second assumption, the dynamic peak current estimation only needs to consider the junction temperatures of the IGBTs and can neglect the junction temperatures of the diodes. The third assumption holds, because the IGBT only conducts during during one half of the excitation period if the current polarity is positive. In this conduction interval, the switching losses are directly proportional to the current and thus track its sinusoidal shape. The conduction losses show a similar characteristics if no strong reduction of the power factor occurs.

Following assumption 3, equation (3) is used to model the device losses of one IGBT such that they are approximated by a sinusoidal half-wave..

$$P_{\mathrm{loss}}^{\mathrm{IGBT}} = \begin{cases} P_{\mathrm{loss}}^{\mathrm{max}} \cdot \sin(\omega_{\mathrm{ex}} t) & \text{if } 2\pi k < \omega_{\mathrm{ex}} t \leq (2k+1)\cdot\pi \\ 0 & \text{if } (2k-1)\cdot\pi < \omega_{\mathrm{ex}} t < 2\pi k \end{cases} \tag{3}$$

The losses are plotted normalized to their peak value as a dashed line in Fig. 5. Note that Fig. 5 has not only a

normalized y-axis, but also a time-axis that is normalized to the excitation period T_{ex}. Next, the junction temperature trace for a sinusoidal loading of the converter is computed for a wide range of excitation frequencies with the derived thermal model. In the Laplace domain, the junction temperature $T_{\mathrm{j}}(s)$ is obtained as a function of the fluid temperature $T_{\mathrm{f}}(s)$, the losses $P_{\mathrm{loss}}(s)$ and the thermal impedance $Z_{\mathrm{th}}(s)$ (4)

$$T_{\mathrm{j}}(s) = T_{\mathrm{f}}(s) + P_{\mathrm{loss}}(s) \cdot Z_{\mathrm{th}}(s) \tag{4}$$

Transformation in the time domain yields the junction temperature response plots that are shown normalized in Fig. 5 for different excitation frequencies.

Fig. 5 shows that the average value of the junction temperature over one excitation period is constant. However, the temperature peak depends strongly on the excitation frequency, because of the thermal capacitance that is embedded in the power module assembly. The junction temperature response at low excitation frequencies $f_{\mathrm{ex}} < 0.1\,\mathrm{Hz}$ shows a peak $T_{\mathrm{j}}^{\mathrm{max}}$ that can be determined assuming a thermal steady-state condition on the basis of the peak losses $P_{\mathrm{loss}}^{\mathrm{max}}$, the thermal resistance of the power module R_{th} and the coolant temperature T_{f} via (5).

$$T_{\mathrm{j}}^{\mathrm{max}}\Big|_{f_{\mathrm{ex}}\to 0} = P_{\mathrm{loss}}^{\mathrm{max}} \cdot R_{\mathrm{th}} + T_{\mathrm{f}} \tag{5}$$

Only the thermal resistance, in case of the Hybridpack2 power module $R_{\mathrm{th}} = 75\,\mathrm{K\,kW^{-1}}$, determines the ratio between peak temperature and losses $\mathrm{d}T_{\mathrm{j}}^{\mathrm{max}}/\mathrm{d}P_{\mathrm{loss}}^{\mathrm{max}} = R_{\mathrm{th}}$. At higher excitation frequencies, the peak temperature reduces due to the thermal capacitances of the lateral structures within the power module. This effect becomes plausible in Fig. 3, that shows how the thermal impedance magnitude decays at higher bandwidth. In case of the Hybridpack2 power module, the junction temperature peak vanishes entirely at excitation frequencies above 200 Hz. At this operation, the maximal junction temperature is reduced by a factor of three compared to the maximal junction temperature that occurs at low excitation frequencies. This factor is obtained because it is the ratio between the average losses and the peak losses $P_{\mathrm{loss}}^{\mathrm{max}}/P_{\mathrm{loss}}^{\mathrm{avg}} = \pi \approx 3$. Following this, the maximal junction temperature at high excitation frequencies can be determine based on (6)

$$T_{\mathrm{j}}^{\mathrm{max}}\Big|_{f_{\mathrm{ex}}\to \infty} = \frac{P_{\mathrm{loss}}^{\mathrm{max}} \cdot R_{\mathrm{th}}}{\pi} + T_{\mathrm{f}} \tag{6}$$

This shows that at rising excitation frequency the thermal characteristics of the power module allow to operate at up to 3 times the peak losses and thus peak current compared to dc operation, without hitting a defined maximal junction temperature level.

B. Dynamic Peak Current Estimation and Control

Now, the dynamic peak current estimation and control is derived that addresses the following opportunities: The power converter can process more current without violating thermal limits if the excitation frequency increases or if the coolant temperature reduces. For this purpose, the maximal feasible converter current amplitude must be derived as a function

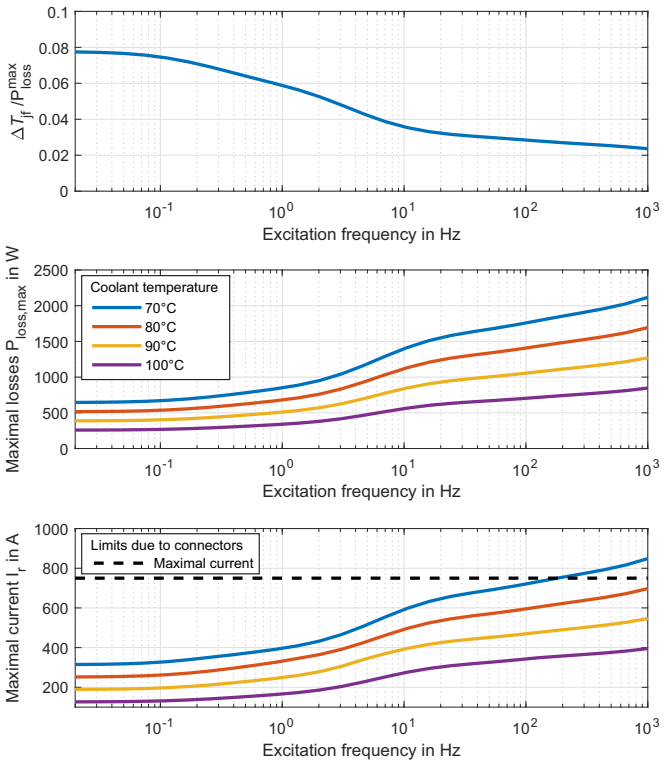

Fig. 6. Maximal junction-to-coolant temperature normalized to the peak of the power half-wave (up), Maximal permissible peak losses at $T_{\mathrm{j}}^{\mathrm{max}} = 120\,^{\circ}\mathrm{C}$ (middle), Maximal feasible peak current amplitude (bottom)

of the excitation frequency and the coolant temperature. In a first step, the maximal temperature drop between junction and coolant $\Delta T_{\mathrm{jf}} = T_{\mathrm{j}} - T_{\mathrm{f}}$ per loss amplitude $P_{\mathrm{loss}}^{\mathrm{max}}$, which is shown for selected excitation frequencies in Fig. 5, is determined at each excitation frequency. The upper trace in Fig. 6 shows this temperature drop ΔT_{jf} that decays at rising excitation frequencies f_{ex}. From this information the maximal feasible loss amplitude can be derived for a given coolant temperatures and a maximal tolerable junction temperature. The middle plot of Fig. 6 depicts exemplary the maximal loss amplitude that ensures a junction temperature below $120\,^{\circ}\mathrm{C}$ as a function of the excitation frequency and the coolant temperature. The maximal feasible current amplitude $I_{\mathrm{r}}^{\mathrm{max}}$ can be derived from this information with a loss model, for the operating point, i.e. modulation index and power factor, at which the maximal losses occur. This current $I_{\mathrm{r}}^{\mathrm{max}}$ is plotted in the lower trace of Fig. 6 with limits that results from the connectors and bond wires, whose temperature also imposes limits.

The dynamic peak current control that together with the thermal monitoring system creates the thermal management solution follows exactly this procedure. Its state-block diagram is shown in Fig. 4. It requires the coolant temperature estimate $\hat{T}_{\mathrm{f}}$, the maximal permissible junction temperature $T_{\mathrm{j}}^{\mathrm{max}}$ and the excitation frequency f_{ex} to determine the peak losses $P_{\mathrm{loss}}^{\mathrm{max}}$ and consequently determine the peak current $I_{\mathrm{r}}^{\mathrm{max}}$. To prevent over temperature, the junction temperature estimate

TABLE I
PARAMETERS OF A PERMANENT MAGNET SYNCHRONOUS DRIVE THAT IS OPERATED WITH/WITHOUT THERMAL MANAGEMENT

Parameter	Value
Power P	175 kW
Motor current $I_{\mathrm{m,max}}$	750 A
PM flux linkage λ_{pm}	0.32 V s
Inductance L_{m}	0.53 mH
Pole pairs p	1
DC-link voltage U_{dc}	400 V

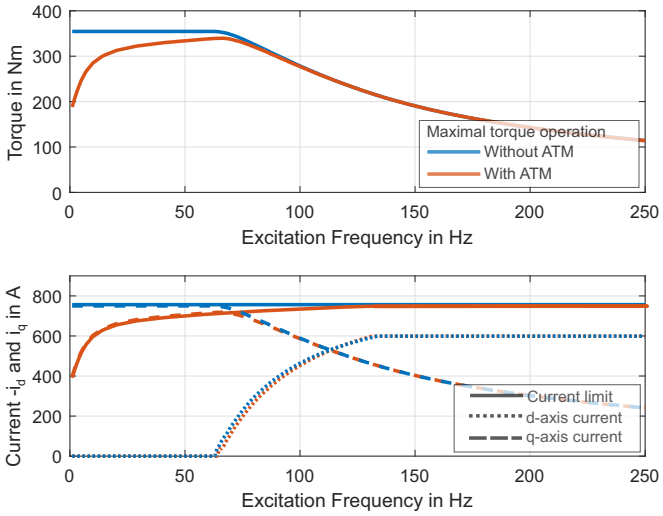

Fig. 7. Drive train operation with static current limit at $I_{\mathrm{max}} = 750\,\mathrm{A}$ and dynamic current limit that is estimated by active thermal management assuming that enforces $T_{\mathrm{j,max}} = 120\,^{\circ}\mathrm{C}$ an operates at $T_{\mathrm{f}} = 70\,^{\circ}\mathrm{C}$

of the thermal monitoring is compared with its maximal value. If over-temperature operation is detected, the peak loss estimation introduces and additional margin to ensure safe operation. The derived maximal current is fed back to the drive control, where it is used as a dynamic current limit, whose effectiveness for increasing the power rating of electrical drive trains is analyzed in the following.

V. Drive Control with Active Thermal Management

The potential of such an active thermal management (ATM) in an electrical drive systems has been evaluated for an example application, whose parameters are summarized in Tab. I. First, the conventional operation of the electrical drives train without active thermal management is considered. In this case, the drive is operated with a converter that can supply a maximal static current of 750 A. The available maximal torque at each excitation frequency and the required d- and q-current are plotted in Fig. 7. This operation requires a comparatively large automotive power module that is able operate at PWM operation with a dc-current of 750 A. As an alternative, the Hybridpack2 power module, whose thermal model was introduced in this paper, is operated with the active thermal management such that the junction temperature does not exceed 120 °C. The red plot in Fig. 7 shows that the

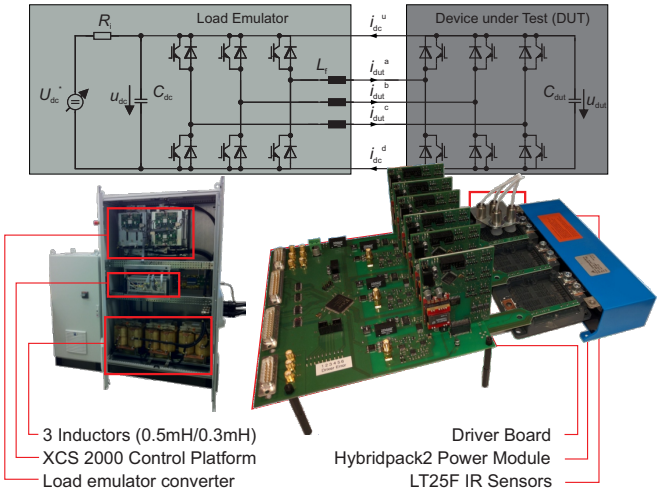

Fig. 8. Experimental setup of the three-phase load emulator with device-under-test based on the Hybridpack2 power module

power module can only operate with a current of 400 A at an excitation frequency of $\omega_{\mathrm{ex}} = 0$. However, the active thermal management allows increasing the operation current at higher excitation frequencies such that the same rated torque at the corner point is realizes that otherwise required a larger power module. Thus, the active thermal management can operate a drive train with smaller more compact power modules without reducing the peak power rating of the drive. Note that in this example only a 100 % overload operation was feasible, because power module connectors only allow operation up to 750 A. However, in general the active thermal management enables overload operation up to 200 % with a suitable packaging technology.

VI. Experimental Results

The introduced active thermal management has been experimentally evaluated with a Hybridpack2 power module on a 3-phase load emulator introduced in [51] that is depicted in Fig. 8. The active thermal management algorithms were implemented of a Shark DSP from Analog Devices and operated at a sampling frequency of 1 kHz. This sampling frequency provides a good compromise between temporal quantization and computation efficiency. For the evaluation shown in Fig. 9, the power module was initially operated at an excitation frequency of 0.1 Hz and at a current of 200 A that was determined to keep the peak junction temperature bellow an exemplary reference value of 40 °C. The excitation frequency was step-wise increased to 20 Hz while the active thermal management operated the converter at the maximal feasible current that did not exceed the reference temperature.

In a second experiment, the converter was operated at varying coolant temperatures, as shown in Fig. 10. During this test, the active thermal management limited the current such that the reference temperature set to 45 °C was not exceeded.

VII. Conclusions

This work introduces an active thermal management system for dynamic peak current control of IGBT inverters. It operates

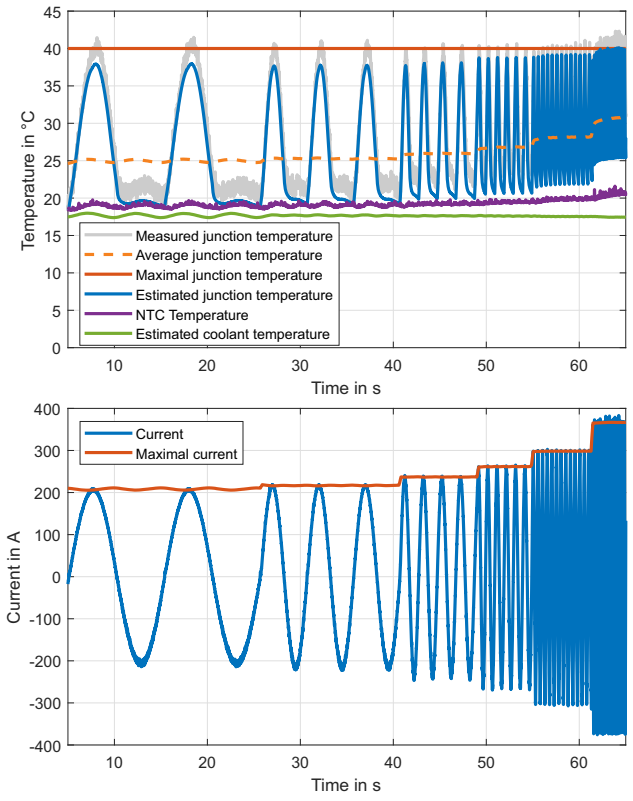

Fig. 9. Operation of an IGBT within a 3-phase PWM inverter at dynamic current limits during a ramp of excitation frequency

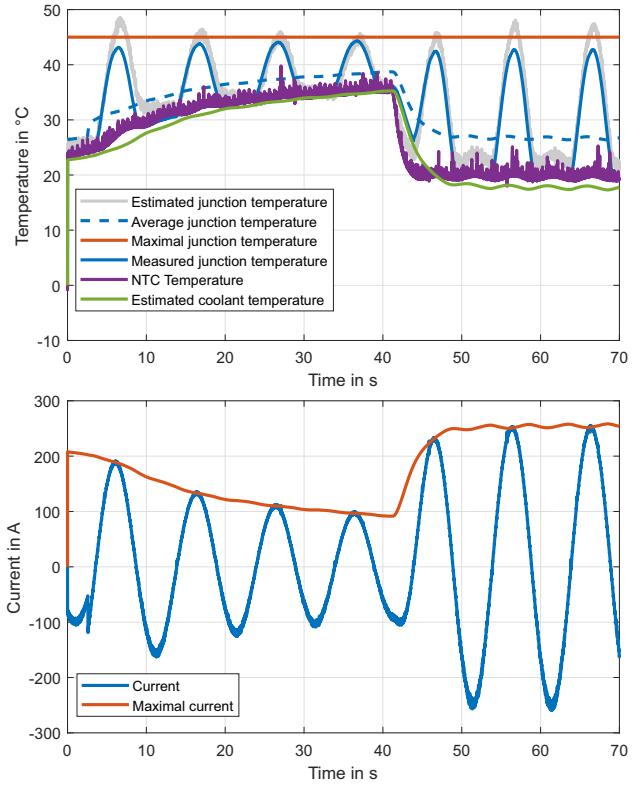

Fig. 10. Operation of an IGBT within a 3-phase PWM inverter at dynamic current limits when the coolant temperature changes

power electronic converters safely at their thermal limits and fully utilize their thermal capability. The active thermal management system has a huge impact at elevated excitation frequencies, as it uses the available thermal capacitance of the converter to increase peak power. Thereby, it allows operating converters at up to 200 % overrating. This provides a huge potential for the integration of power converters in electrical drives trains reducing space, volume and costs.

REFERENCES

[1] A. Sewergin, A. Stippich, and A. H. W. R. W. D. Doncker, "Comparison of high performance cooling concepts for SiC power modules," in *2019 IEEE Applied Power Electronics Conference and Exposition (APEC)*, IEEE, Mar. 2019.

[2] A. Stippich, C. H. van der Broeck, A. Sewergin, A. H. Wienhausen, M. Neubert, P. Schülting, S. Taraborrelli, H. van Hoek, and R. W. De Doncker, "Key components of modular propulsion systems for next generation electric vehicles," *CPSS Transactions on Power Electronics and Applications*, vol. 2, no. 4, pp. 249–258, Dec. 2017.

[3] M. Rosekeit, C. H. van der Broeck, and R. W. De Doncker, "Dynamic control of a dual active bridge for bidirectional ac charging," in *2015 IEEE International Conference on Industrial Technology (ICIT)*, IEEE, Mar. 2015, pp. 2085–2091.

[4] A. Merkert, T. Krone, and A. Mertens, "Characterization and scalable modeling of power semiconductors for optimized design of traction inverters with si- and SiC-devices," *IEEE Trans. on Power Electr.*, vol. 29, no. 5, pp. 2238–2245, May 2014.

[5] A. H. Wienhausen, A. Sewergin, and R. W. De Doncker, "Highly compact galvanically coupled dc/dc converters for modular drive trains," in *10th Expert Forum Electric Vehicle Drives*, 2018.

[6] C. Neeb, L. Boettcher, M. Conrad, and R. De Doncker, "Innovative and reliable power modules: A future trend and evolution of technologies," *Industrial Electronics Magazine, IEEE*, vol. 8, no. 3, pp. 6–16, Sep. 2014.

[7] M. Conrad, R. W. De Doncker, M. Schniedenharn, and A. Diatlov, "Packaging for power semiconductors based on the 3d printing technology selective laser melting," in *European Conference on Power Electronics and Applications*, IEEE, Aug. 2014.

[8] A. H. Wienhausen, A. Sewergin, S. P. Engel, and R. W. De Doncker, "Highly efficient power inductors for high-frequency wide-bandgap power converters," in *IEEE International Conference on Power Electronics and Drive Systems (PEDS)*, IEEE, Dec. 2017.

[9] C. H. van der Broeck, T. Polom, R. D. Lorenz, and R. W. De Doncker, "Real-time monitoring of thermal response and life-time varying parameters in power modules," *IEEE Transactions on Industry Applications*, 2020.

[10] Y. Avenas, L. Dupont, N. Baker, H. Zara, and F. Barruel, "Condition monitoring: A decade of proposed techniques," *IEEE Industrial Electronics Magazine*, vol. 9, no. 4, pp. 22–36, Dec. 2015.

[11] C. H. van der Broeck, S. Kalker, T. A. Polom, W. De Doncker, and L. R. D., "In-situ thermal impedance spectroscopy of power electronic modules for localized degradation identification," in *International Exhibition and Conference for Power Electronics, Intelligent Motion, Renewable Energy and Energy Management (PCIM Europe)*, 2019.

[12] T. A. Polom, R. D. Lorenz, C. H. van der Broeck, and R. W. De Doncker, "Designing power modules for degradation sensing," in *2019 IEEE Energy Conversion Congress and Exposition (ECCE)*, 2019.

[13] G. Moreno, "Gaining traction: Thermal management and reliability of automotive electric traction-drive systems," *IEEE Electrification Magazine*, vol. 2, no. 2, pp. 42–49, Jun. 2014.

[14] A. Stippich, M. Battefeld, and R. W. De Doncker, "Integrated cooling channels in direct bonded copper substrates for silicon carbide mosfets," englisch, in *International Exhibition and Conference for Power Electronics, Intelligent Motion, Renewable Energy and Energy Management (PCIM)*, Nuremberg: VDE, Jun. 2018, pp. 1400–1407.

[15] M. Andresen, K. Ma, G. Buticchi, J. Falck, F. Blaabjerg, and M. Liserre, "Junction temperature control for more reliable power electronics," *IEEE Transactions on Power Electronics*, vol. 33, no. 1, pp. 765–776, Jan. 2018.

[16] T. A. Polom, B. Wang, and R. D. Lorenz, "Control of junction temperature and its rate of change at thermal boundaries via precise loss manipulation," *IEEE Transactions on Industry Applications*, vol. 53, no. 5, pp. 4796–4806, Sep. 2017.

[17] V. Blasko, R. Lukaszewski, and R. Sladky, "On line thermal model and thermal management strategy of a three phase voltage source inverter," in *Industry Applications Conference, 1999*, vol. 2, 1999, 1423–1431 vol.2.

[18] L. Wei, J. McGuire, and R. A. Lukaszewski, "Analysis of pwm frequency control to improve the lifetime of pwm inverter," *IEEE Transactions on Industry Applications*, vol. 47, no. 2, pp. 922–929, Mar. 2011.

[19] D. A. Murdock, J. E. R. Torres, J. J. Connors, and R. D. Lorenz, "Active thermal control of power electronic modules," *IEEE Transactions on Industry Applications*, vol. 42, no. 2, pp. 552–558, Mar. 2006.

[20] M. Andresen, G. Buticchi, J. Falck, M. Liserre, and O. Muehlfeld, "Active thermal management for a single-phase h-bridge inverter employing switching frequency control," in *PCIM Europe 2015*, May 2015, pp. 1–8.

[21] H. Luo, F. Iannuzzo, K. Ma, F. Blaabjerg, W. Li, and X. He, "Active gate driving method for reliability improvement of igbts via junction temperature swing reduction," in *Symposium on Power Electronics for Distributed Generation Systems (PEDG)*, 2016.

[22] C. H. van der Broeck, L. A. Ruppert, R. D. Lorenz, and R. W. De Doncker, "Active thermal cycle reduction of power modules via gate resistance manipulation," in *2018 IEEE Applied Power Electronics Conference and Exposition (APEC)*, IEEE, Mar. 2018.

[23] C. Lüdecke, F. Krichel, M. Laumen, and R. W. De Doncker, "Balancing the switching losses of paralleled SiC MOSFETs using an intelligent gate driver," in *International Exhibition and Conference for Power Electronics, Intelligent Motion, Renewable Energy and Energy Management (PCIM Asia)*, VDE, Nov. 2020.

[24] Y. Yerasimou, V. Pickert, B. Ji, and X. Song, "Liquid metal magnetohydrodynamic pump for junction temperature control of power modules," *IEEE Transactions on Power Electronics*, vol. PP, no. 99, pp. 1–1, 2018.

[25] C. Li, D. Jiao, J. Jia, F. Guo, and J. Wang, "Thermoelectric cooling for power electronics circuits: Modeling and active temperature control," *IEEE Transactions on Industry Applications*, vol. 50, no. 6, pp. 3995–4005, Nov. 2014.

[26] Y. Ko, M. Andresen, G. Buticchi, and M. Liserre, "Discontinuous modulation based active thermal control of power electronic modules in wind farms," *IEEE Transactions on Power Electronics*, pp. 1–1, 2018.

[27] C. H. van der Broeck, L. A. Ruppert, R. D. Lorenz, and R. W. A. De Doncker, "Methodology for active thermal cycle reduction of power electronic modules," *IEEE Transactions on Power Electronics*, 2018.

[28] J. Ewanchuk, J. Brandelero, and S. Mollov, "Lifetime extension of a multi-die sic power module using selective gate driving with temperature feedforward compensation," in *2017 IEEE Energy Conversion Congress and Exposition (ECCE)*, Oct. 2017, pp. 2520–2526.

[29] C. H. van der Broeck and R. W. De Doncker, "Thermal monitoring of power electronic modules with minimal sensing effort," in *2019 IEEE Energy Conversion Congress and Exposition (ECCE)*, 2019.

[30] N. Baker, S. Munk-Nielsen, F. Iannuzzo, and M. Liserre, "Igbt junction temperature measurement via peak gate current," *IEEE Transactions on Power Electronics*, vol. 31, no. 5, pp. 3784–3793, May 2016.

[31] C. H. van der Broeck, A. Gospodinov, and R. W. De Doncker, "IGBT junction temperature estimation via gate voltage plateau sensing," *IEEE Transactions on Industry Applications*, pp. 1–1, Sep. 2018.

[32] H. Niu and R. D. Lorenz, "Evaluating different implementations of online junction temperature sensing for switching power semiconductors," *IEEE Transactions on Industry Applications*, vol. 53, no. 1, pp. 391–401, Jan. 2017.

[33] S. Kalker, C. H. van der Broeck, and R. W. De Doncker, "Online junction-temperature sensing of sic mosfets with minimal calibration effort," in *PCIM Europe 2020; International Exhibition and Conference for Power Electronics, Intelligent Motion, Renewable Energy and Energy Management*, May 2020.

[34] J. Winkler, J. Homoth, and I. Kallfass, "Electroluminescence-based junction temperature measurement approach for SiC power MOSFETs," *IEEE Transactions on Power Electronics*, vol. 35, no. 3, pp. 2990–2998, Mar. 2020.

[35] C. H. van der Broeck, R. D. Lorenz, and R. W. A. De Doncker, "Monitoring 3-d temperature distributions and device losses in power electronic modules," *IEEE Transactions on Power Electronics*, 2018.

[36] C. H. van der Broeck, T. Polom, R. D. Lorenz, and R. W. De Doncker, "Thermal monitoring of power electronic modules via device self-sensing," in *2018 IEEE Energy Conversion Congress and Exposition (ECCE)*, Sep. 2018.

[37] J. Ruthardt, P. Ziegler, M. Fischer, and J. Roth-Stielow, "Model based junction temperature control using the gate driver voltage as a correction variable," in *2019 21st European Conference on Power Electronics and Applications (EPE '19 ECCE Europe)*, IEEE, Sep. 2019.

[38] F. Hahn, M. Andresen, G. Buticchi, and M. Liserre, "Thermal analysis and balancing for modular multilevel converters in hvdc applications," *IEEE Transactions on Power Electronics*, vol. 33, no. 3, pp. 1985–1996, Mar. 2018.

[39] A. Wintrich, U. Nicolai, W. Tursky, and T. Reimann, *Application Manual Power Semiconductors*, S. I. GmbH, Ed. ISLE Verlag, 2015.

[40] C. H. van der Broeck, M. Conrad, and R. W. De Doncker, "A thermal modeling methodology for power semiconductor modules," *Microelectronics Reliability*, vol. 55, no. 9-10, pp. 1938–1944, Aug. 2015.

[41] C. H. van der Broeck, L. A. Ruppert, A. Hinz, M. Conrad, and R. W. De Doncker, "Spatial electro-thermal modeling and simulation of power electronic modules," *IEEE Transactions on Industry Applications*, vol. 54, no. 1, pp. 404–415, Jan. 2018.

[42] T. Polom, C. H. van der Broeck, R. W. De Doncker, and R. D. Lorenz, "Real-time, in situ degradation monitoring in power semiconductor converters," in *2018 IEEE Applied Power Electronics Conference and Exposition (APEC)*, 2019.

[43] T. A. Polom, C. H. van der Broeck, D. D. R. W., and L. R. D., "Spatially-varying electrothermal impedance analysis for designing power semiconductor converter systems," in *Intersociety Conference on Thermal and Thermomechanical Phenomena in Electronic Systems (ITherm)*, 2019.

[44] F. Qi, D. A. Ly, C. H. van der Broeck, D. Yan, and R. W. De Doncker, "Model order reduction suitable for online linear parameter-varying thermal models of electric motors," in *2016 IEEE 2nd Annual Southern Power Electronics Conference (SPEC)*, IEEE, Dec. 2016, pp. 1–6.

[45] T. A. Polom, M. Andresen, M. Liserre, and R. D. Lorenz, "Frequency-domain electrothermal impedance spectroscopy of an actively switching power semiconductor converter," *IEEE Transactions on Industry Applications*, vol. 55, no. 6, pp. 6161–6172, 2019.

[46] K. Ma, N. He, M. Liserre, and F. Blaabjerg, "Frequency-domain thermal modeling and characterization of power semiconductor devices," *IEEE Transactions on Power Electronics*, vol. 31, no. 10, pp. 7183–7193, Oct. 2016.

[47] N. Baker, M. Liserre, L. Dupont, and Y. Avenas, "Improved reliability of power modules: A review of online junction temperature measurement methods," *IEEE Industrial Electronics Magazine*, vol. 8, no. 3, pp. 17–27, Sep. 2014.

[48] C. Kempiak, A. Lindemann, E. Thal, and S. Idaka, "Investigation of the usage of a chip integrated sensor to determine junction temperature during power cycling tests," in *CIPS 2018; 10th International Conference on Integrated Power Electronics Systems*, Mar. 2018, pp. 1–6.

[49] S. Kalker, C. H. van der Broeck, and De Doncker, "Utilizing electroluminescence of sic mosfets for unified junction-temperature and current sensing," in *2020 IEEE Applied Power Electronics Conference and Exposition (APEC)*, 2020.

[50] C. H. van der Broeck, R. D. Lorenz, and R. W. De Doncker, "Methods for monitoring 3-d temperature distributions in power electronic modules," in *2018 IEEE Applied Power Electronics Conference and Exposition (APEC)*, IEEE, Mar. 2018.

[51] C. H. van der Broeck, H. Zeng, R. D. Lorenz, and R. W. De Doncker, "A test bench for thermal characterization of igbt power modules over mission profiles," in *PCIM Europe 2018; International Exhibition and Conference for Power Electronics, Intelligent Motion, Renewable Energy and Energy Management*, Jun. 2018.